Nuclear Physics A520 (1990) 153c-168c
North-Holland

Alpha-Particle Emission as a Probe of Nuclear Shapes and Structure Effects in Proton Evaporation Spectra

N.G. Nicolis[1], D.G. Sarantites[1], C. Baktash[2], V. Abenante[1], L.A. Adler[1], J.R. Beene[2], F.A. Dilmanian[1], G. Garcia-Bermudez[2], H.C. Griffin[3], M.L. Halbert[2], D.C. Hensley[2], N.R. Johnson[2], I.Y. Lee[2], Z. Majka[1], F.K. McGowan[2], M.A. Riley[2], T.M. Semkow[1], D.W. Stracener[1], and A. Virtanen[2]

[1] *Department of Chemistry, Washington University, St. Louis, MO 63130*
[2] *Physics Division, Oak Ridge National Laboratory, Oak Ridge, TN 37831*
[3] *Department of Chemistry, University of Michigan, Ann Arbor, MI 48109*

Emission barriers and subbarrier anisotropies from α decay of Sn* and Yb* compound nuclei are examined in the light of calculations incorporating deformation effects in the decay process. For the Yb* systems deformation which increases with spin is necessary to explain the data. For the Sn* systems the spectral shapes and anisotropies can be explained without deformation. For systems lighter than Sn this probe is not sensitive to the deformation. Energy spectra and angular correlations of evaporated protons from the ^{52}Cr(^{34}S, 2n2p)^{82}Sr reaction were measured in coincidence with discrete transitions. Large shifts in proton spectra were observed when high spin states in different rotational bands are populated. They are interpreted as due to near-yrast stretched proton emission preferentially populating the yrast band by subbarrier protons. Simulations show that channel selected proton spectra cannot be used as probes of deformation.

1. Introduction

In recent years, there has been a considerable interest in the study of nuclear shapes at high excitation and angular momentum. It is well established that collective nuclei near the yrast line are deformed, and that their structure is well described by liquid-drop-Strutinsky cranked shell model calculations. Temperature-induced noncollective rotation in nuclei has been discussed with equilibrium shapes described by mean field theories, such as the finite-temperature Hartree-Fock-Bogoliubov crancking theory.[1] As the temperature is increased at constant spin a phase transition may occur from prolate to oblate shapes. Thus, for spin 40$\hbar$, this is predicted to occur in ^{166}Er at a temperature of 1.64 MeV.[2] Numerous experimental studies have addressed the issue of the effect of excitation energy and spin on the nuclear shapes. One of the probes utilizes the decay of the giant dipole resonances built on excited states.[3,4] Another probe involves the utilization of charged particle decay in order to find signatures of shape effects in the shape of the particle spectra for such systems.[5-11]

The interest in using the charged particles as a probe of deformation relies on the fact that a lower evaporation barrier along the longer axis should favor particle emission in that direction compared with the spherical case. This results in strong enhancements of α and proton emission along the long axis, especially for the region below the evaporation

Coulomb barrier.[5,6,12] The inability to reproduce the sub-barrier portion of the α-particle spectra with statistical model calculations assuming spherical emission shapes, has been used as evidence for deformation.

Assuming that the shape fluctuations due to thermal effects do not wash out the correlation between the symmetry and the rotation axes, we would expect larger anisotropies along the direction perpendicular to the spin for prolate nuclei rotating perpendicular to the symmetry axis, or for oblate nuclei rotating along the symmetry axis. This has led to the development of the spin alignment method with the Spin Spectrometer, allowing measurements of the α angular distributions with respect to the spin direction to be made.[13,14]

In Section 2 we discuss sub-barrier α emission as a probe of nuclear deformation at high spins and excitations. In Section 3 we discuss nuclear structure and deformation effects on the shape of proton evaporation spectra.

2. Deformation Effects on Alpha Emission Properties.

The interpretation of charged-particle evaporation spectra requires a careful treatment of the light particle emission properties in the statistical model description. The comparison of our experimental data with the statistical model calculations, presented below, was made with the Monte-Carlo evaporation code PACEX[18]. This code was obtained from the code PACE[19] after extensive corrections and extensions. The modifications relevant to the present work have been published[9,11] and are described briefly below.

According to the statistical model, the particle emission rate is proportional to

$$\rho(E^* - E_{rot} - \Delta) \cdot \Sigma_\ell T_\ell(\epsilon).$$

The first term is the level density of the available final states and the second one is the penetrability term, which determines the access to the phase space described by the level density. The quantity E_{rot} describes the yrast lines up to spins where discrete levels are known. For the higher spins we matched the experimental yrast lines to those from the rotating liquid drop model with finite range corrections. Odd mass yrast lines were also shifted to match the experimental ones. This procedure introduces some of the effects of dependence in the level density on deformation which is naturally present in the yrast lines constructed as discussed above. The expression for the $E1$ γ-ray emission includes the giant dipole resonance (GDR) term. The shape and position of the GDR are taken taken from systematics[20,21] and the strength is determined by the energy weighted sumrule.[20] The GDR splittings due to deformation were included using a double Lorenzian shape parametrization. Statistical $E1$ and $M1$ transitions as well as collective stretched E2 transitions for $E_\gamma \leq 2$ MeV were included (further details are given in Ref. 9).

For the calculations for spherically symmetric systems, transmission coefficients for charged particle emission were obtained from optical model calculations with the parameters of Willmore and Hodgson[22] and of Perey and Perey[23] for the neutrons and protons, respectively. For the α-particles, we have chosen the optical model parameters of McFadden and Satchler.[24] Complete optical model calculations were performed for isotopes in 20 × 10 (N,Z) grids which span the range of isotopes considered in each statistical model calculation. Theses sets of transmission coefficients were stored in computer files to be used by PACEX. This procedure is free of the previously employed approximations, where extrapolations were used to determine transmission coefficients in the later stages of the deexcitation. In particular, this modification makes the code applicable in studies of medium to light deexciting compound systems where the old method produced "artificial" subbarrier alphas[25].

The effects of deformation were introduced in the penetrability term in the following way. The daughter nuclei were assumed to have an axially symmetric prolate shape, which was parameterized in terms of the quadrupole deformation parameter β_2 as

$$R(\theta) = R_0\,[1 + X(\beta_2) + \sqrt{5/4\pi}\beta_2 P_2(cos\,\theta)] \qquad (1)$$

where θ is the angle with respect to the symmetry axis and $X(\beta_2)$ is the volume conservation term. Optical model transmission coefficients for protons and alphas were calculated for all nuclei in the cascade at nine different angles θ from 5° to 85° in steps of 10°. For each angle, the optical model radii were scaled according to eq. (1). The diffuseness of the Woods-Saxon nuclear potential of the spheroid was modified, so that the normal derivative at each point on the equipotential surface is unaffected by the deformation. The above transmission coefficients were stored in computer files and read in by PACEX. Each angle θ was sampled by a random number choice weighted according to the surface element of the spheroid: $2\pi R^2(\theta) sin\theta \Delta\theta / S$ where S is the nuclear surface including a correction due to deformation. This selects the transmission coefficients at the appropriate position on the nuclear surface for each event. Using the above method, the effect of deformation becomes apparent in the sub-barrier region of the particle spectra.

The compound nuclei studied in this work were ^{114}Sn*, ^{134}Nd*, ^{164}Yb* and ^{170}Yb*. These were produced in the reactions ^{64}Ni (250 MeV) + ^{50}Ti $\rightarrow$ ^{114}Sn* (79.5 MeV, 65.3$\hbar$), ^{64}Ni (270 MeV) + ^{74}Ge $\rightarrow$ ^{138}Nd* (82.4 MeV, 79.1$\hbar$), ^{64}Ni (270 MeV) + ^{100}Mo $\rightarrow$ ^{164}Yb* (67.2 MeV, 73.6 $\hbar$), and ^{20}Ne (176.6 MeV) + ^{150}Nd $\rightarrow$ ^{170}Yb* (134.8 MeV, 76.6$\hbar$), where the numbers in parentheses are the initial excitation energy and the critical angular momentum. The experiments were performed at the Oak Ridge Holifield heavy Ion Research Facility. The α-particle spectra were recorded with Si surface barrier telescopes positioned at laboratory angles close to those corresponding to 90° in the center of mass. The α particles were recorded in coincidence with the Spin Spectrometer which provided the

associated γ-ray multiplicity, M_γ, and the angle of emission with respect to the estimated spin direction.[13,14] Full details of the experimental methods have been presented in Ref. 9.

Below, we compare the experimental with calculated α particle evaporation spectra and angular correlations with statistical model calculations. We place particular emphasis in analyzing systems for which the ℓ_{cr} values are derived from experimental cross sections for evaporation residues (σ_{ER}), and for which cross sections to individual exit channels such as (HI, αxn) and (HI, xn) have been measured and can be reproduced by the calculations.

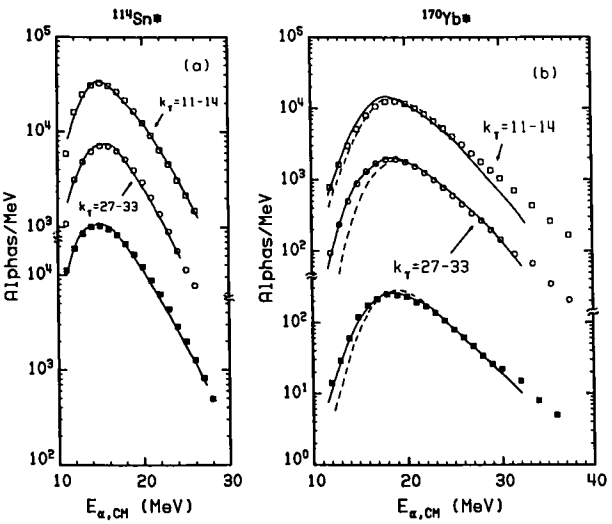

Figure 1. (a) γ-fold gated 90° center-of-mass α-particle spectra from the deexcitation of ^{114}Sn*. The open squares correspond to k_γ = 11–14 and the open circles to k_γ = 27–33. The closed squares show the 90° center-of-mass spectrum integrated over k_γ ($k_\gamma > 10$) and the angle with respect to the spin direction. (b) γ-fold gated 90° center-of-mass alpha-particle spectra from ^{170}Yb*. The squares correspond to k_γ = 11–14 and the circles to k_γ = 27–33. The closed squares show the 90° center-of-mass spectrum integrated over k_γ ($k_\gamma > 10$) and the angle with respect to the spin direction. The solid and dashed lines are the results of calculations described in the text.

For the calculations with spherically symmetric parameters, transmission coefficients were generated withe the above referenced optical model parameter sets. This choice was made on the basis of (a) an overall better agreement of the sub-barrier part of the α spectrum and of the α anisotropies for the Sn* systems, and (b) a better description of fusion data of alpha particles on targets with mass close to the compound nuclei of Yb*.

In fig. 1 the open squares, open circles, and full squares give the α-spectra emitted at 90° in the center of mass system gated by a γ-ray coincidence fold, k_γ, in the range 11–14, 27–33, and $k_\gamma > 10$, respectively. The spectra from Figs. 1(a) and 1(b) are from the ^{114}Sn* and ^{170}Yb* decays, respectively. We note that the shape of these evaporative spectra does not change significantly with k_γ and therefore spin. However, a close examination of the spectra from ^{114}Sn* reveals that the spectrum corresponding to k_γ=11–14 shifts its peak position to lower energy, thus increasing the sub-barrier yield, and it is also harder relative to the k_γ=27–33 spectrum. The above trends are reversed in the case of ^{170}Yb* with respect to the sub-barrier alphas, with the high k_γ spectrum having slightly more

sub-barrier alphas, and the low k_γ spectrum again being harder. The above results are compared first with calculated spectra assuming spherical emission barriers. The solid lines in fig. 1(a) are the calculated spectra for ^{114}Sn* with γ-ray multiplicity gates placed on the PACEX events corresponding to the experimental k_γ gates. It is seen that the α spectra for all k_γ gates are explained well by the calculation without the need to invoke deformation effects. For the ^{170}Yb* system, however, this is not the case. The results of a calculation with the spherical emission barriers are shown in fig. 1(b) by the dashed lines. First, we note that in all cases the sub-barrier region is underpredicted considerably by the spherical calculation. In fact, this underprediction is small for the low k_γ spectrum and very large for the high k_γ spectrum. The underprediction at high E_α for k_γ = 11–14 is due to the presence of some pre-equilibrium α particles. The trends below the barrier can be understood if deformation effects are introduced. The solid lines in fig. 1(b) show the results of such calculations. The solid curve for k_γ=11–14 corresponds to $\beta = 0.2$ and it overpredicts somewhat the sub-barrier spectrum. A value of $\beta \sim 0.15$ gives a better fit to the data. The solid curve for k_γ = 27–33 corresponds to $\beta = 0.35$ and fits the data quite well. For the $k_\gamma > 10$ spectrum an average $\beta = 0.25$ gives the best overall fit. These findings show that the deformation increases with increasing spin, which is consistent with the predictions or rotating liquid drop model. Similar conclusions are reached for the α spectra from ^{164}Yb* while for those from ^{138}Nd* small deformations are required.[9]

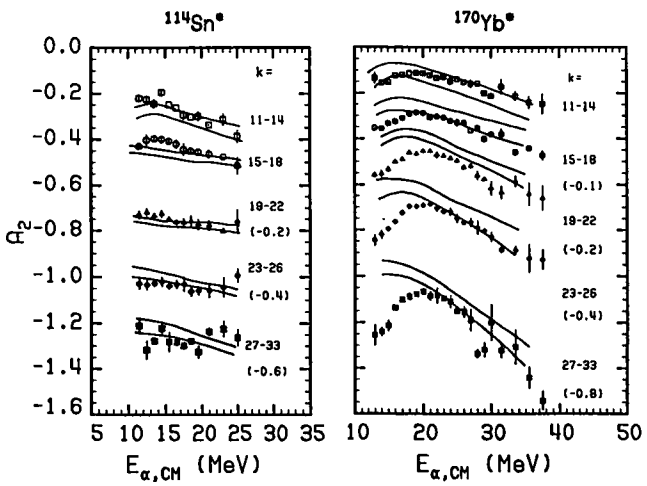

Figure 2. A_2 coefficients as a function of $E_{\alpha,C.M.}$ from the ^{114}Sn* and ^{170}Yb* systems. In both cases, the open squares, circles, full triangles, diamonds and full squares correspond to the k_γ bins of 11–14, 15–18, 19–22, 23–26 and 27–33, corresponding to $< I >_\alpha$ for α emission of 34, 43, 51, 59, and 64 $\hbar$, respectively. In some cases the data have been shifted along the A_2-axis by the indicated amount. The pairs of curves are FWHM boundaries of the A_2 coefficients from a statistical model calculation using transmission coefficients from a spherical optical model potential.

The above findings are further supported by the observed α particle angular correlations.[9] The angular correlations of α particles for each E_α (1 MeV bins) with respect to the estimated spin direction were fitted to the function

$$W(\beta) = A_0[1 + A_2P_2(cos\beta) + A_4P_4(cos\beta)].$$

The A_4 coefficients were found to be small in all of the cases under study and they can be neglected, to first order. The coefficients A_2 from the ^{114}Sn* and ^{170}Yb* systems are shown as the data points in Figs. 2(a) and 2(b) for the five k_γ bins indicated. For the ^{114}Sn* case, the A_2 coefficients show a monotonic dependence becoming less negative as E_α decreases. In contrast, for the ^{170}Yb* system, as E_α decreases the A_2 coefficients first become less negative but at approximately the barrier energy turn and become more negative again. Since a negative A_2 coefficient corresponds to a preferred emission perpendicular to the spin direction, the above downturn below the barrier indicates a stronger preferred emission perpendicular to the spin direction. If the nucleus has a prolate shape and rotates perpendicular to the long axis, then the above effect would be what one would expect, because of the lower barrier in the direction perpendicular to spin. The solid lines in fig. 2 are the calculated A_2 coefficients from a statistical model calculations assuming penetrabilities from a spherical optical potential. The ^{114}Sn* A_2 coefficients are well reproduced by the calculation. For the ^{170}Yb* case, only the high energy dependence is reproduced. Below the barrier, the spherical calculation does not reproduce the enhanced emission perpendicular to the spin direction .[9] In a recent semiclassical calculation, Aleshin[26] has been able to reproduce the downturn in fig. 2(b) assuming a deformation consistent with our earlier findings.

From the above discussion, it is apparent that for the rare earth nuclei the sub-barrier emission of α particles is indeed a good probe for nuclear shapes for excited highly spinning nuclei. This remains true as long as the α particle multiplicity is small and below unity. It is therefore interesting to examine the range of excitation energies that is probed by the sub-barrier α emission. Statistical model calculations for the ^{164,170}Yb* cases show that the distributions in excitation energy of the α emitting states shift to lower energies as the E_α decreases below the barrier. Despite this trend, for E_α values where the deformation effects are observed, a broad range of excitation energies is sampled, particularly for emitting states at high spin.[9]

A few comments have to be made on the utility of the α emission as a probe of nuclear shapes in medium to light compound nuclear systems. Recent analyses of α-particle spectra from the light compound ^{60}Ni* system at moderately high excitation (formed in the reaction of 120 MeV ^{30}Si with ^{30}Si) have shown large discrepancies between the experimental and calculated spectra.[15] A good description was proposed[15] with the emission barrier significantly reduced and the entrance channel critical angular momentum decreased below the experimental value. Such modifications in the parameters of the

statistical model calculations suggested emission from an oblate shape with an axis ratio $\approx$ 3:1.[15]. The analysis leading to such unrealistic deformations was criticized by Nicolis and Sarantites[16] who showed that standard analysis with a realistic set of parameters for the evaporation code PACEX reproduced the data of Ref. 15 without the need to introduce deformation. The reason for the originally reported surprisingly large deformations has been traced in the use of simplistic models in the interpretation of the complex decay sequences in these light systems.[17] Critical analyses[17] of α spectra from systems with A $\leq$ 75 did not show the need for introducing deformation, although for some of the systems, deformation effects were introduced by increasing the level density at high spins by lowering the yrast line and using the Fermi gas level density expression.[17] It has also been pointed out[17] that in the lighter systems where many charged particles are emitted the observed spectra are sums of spectra from a large number of decay sequences and this perhaps masks the effect of deformation on the observed spectra. For heavier systems and for moderate excitation energies where the α-particle multiplicity is of the order of 1 or less, these difficulties are avoided.

In conclusion, α-emission below the evaporation barrier is a good probe for nuclear shapes of hot, rapidly rotating nuclei in the rare earth region. For lighter systems in the Sn region or other systems lighter than Sn, this probe is not sensitive to the deformation. The deformations found in the Yb* systems increase with spin in agreement with the liquid drop model. We should point out that this method does not distinguish between prolate and oblate emitting shapes.

3. Nuclear Structure Effects in Proton Evaporation Spectra

Compound nuclei leading to evaporation residues with large deformations may be expected to have significant deformations that can be probed by α particle or proton emission from high excitations. The effect of deformation on proton spectra was one of the aspects in motivating the work reported here. Another interesting aspect was to investigate whether structural effects in the γ de-excitation process preferentially connect certain entry state regions to final states of different structure belonging to different rotational bands in the final nucleus.

In order to explore the above two aspects, we selected for study the final nucleus ^{82}Sr, because it was predicted to be a good candidate for superdeformation.[27] We have observed unexpected large shifts in the proton spectra when high spin states in different rotational bands in ^{82}Sr were populated.

The experiment was performed at the Oak Ridge Heavy Ion Research Facility. The ^{82}Sr nuclei were produced by the ^{52}Cr(^{34}S, 2n2p)^{82}Sr reaction by bombarding a stack of self-supporting ^{52}Cr target foils with a 130 MeV ^{34}S beam. The experimental setup consisted of the ORNL Compton suppression spectrometer with 18 Ge detectors, which recorded the discrete γ-ray spectra from the reaction. The associated γ-ray coincidence

fold, k_γ and total γ-ray energy were recorded with the Spin Spectrometer. The protons and α particles were detected with the 4π CsI(Tl) Dwarf Ball .[28] This system provided both high resolution γ-ray spectroscopic information and definite exit channel selection. The 72-element Dwarf Ball also provided light charged particle spectra and angular correlation information. The apparatus was triggered by any two or more Ge detectors firing in coincidence with any element of the Dwarf Ball. A total of 1.6×10^8 such events were collected and processed.

Using the pulse shape discrimination capabilities of the CsI(Tℓ), excellent separation for all energies was achieved between proton and α pulses from each other and from γ-rays or neutrons for the detectors forward of 102° in the laboratory ($\sim$ 120° center-of-mass). Protons with sub-barrier energies and yields $\sim$ 1/20 of that at the most probable value could be clearly identified . Proton spectra sorted in this way contained $\sim$ 65% of the total proton yield. At larger angles due to kinematic forward focussing a small fraction of the sub-barrier protons cannot be distinguished from α particles and therefore the detectors at these angles were used for channel selection, but not for particle spectra. The measured overall detection efficiency for protons was 85% of 4π (67 detectors out of 72 were used). This resulted in $\sim$ 28% of the events with two protons to be identified as involving only one proton. The Ge energy spectra coincident with 2 protons involved primarily ^{82}Sr γ-rays with no contamination from the 1pxn or the αxn channels. In the most forward detectors the counting rate was $\sim$ 7000 c/s. The Dwarf Ball detectors were calibrated using the ^{12}C(p, p') reaction at 9.0 and 20.0 MeV.

The particle energies were converted event by event to the center-of-mass system. The centroid angles for each detector in the laboratory system were used in deriving the center-of-mass energy and angle, assuming two-body kinematics. Proton energy spectra were sorted using the detectors forward of 102°, when 2 protons were identified in the complete Dwarf Ball and for three k_γ gates of 3–9, 10–14, and 15–25. Further selection was made by placing gates on discrete γ-rays associated with various rotational bands. The background to the proton spectra associated with the underlying Compton contribution in the Ge peaks were subtracted by placing equal width gates near each γ peak. Care was exercised to avoid peaks that are known to be doublets. Thus, for the four main bands, gates placed on single γ-ray peaks for transitions up to spin 10 gave spectra of good statistical quality. For higher spins, the proton spectra for two or three transitions were added to provide spectra of improved statistical quality, but in each case the spectra for each gate were examined for consistency.

Angular correlations of the coincident protons were recorded at 24°, 42°, 50°, 63°, 68°, and 78° in the laboratory, corresponding to angles ranging from $\sim$ 30° to 95° in the center of mass.

The level scheme for ^{82}Sr was constructed from a γ-γ matrix obtained by requiring that at least one proton was detected and that k_γ exceeded 10. The matrix thus constructed was

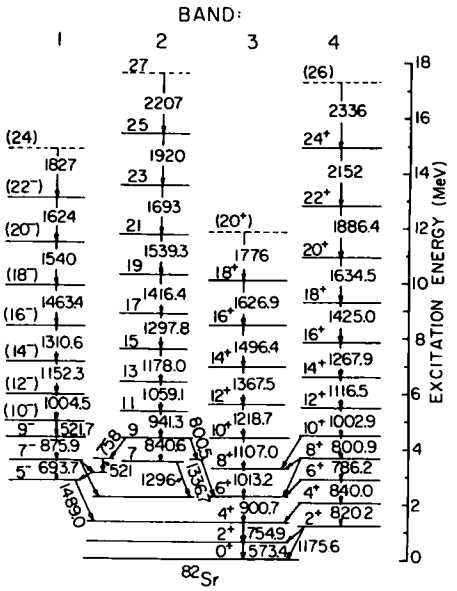

Figure 3. Partial level scheme for ^{82}Sr showing four major rotational bands. Band 3 is the ground band, and band 4 is the yrast one. The odd-spin band 2 becomes yrast at spins higher than 23.

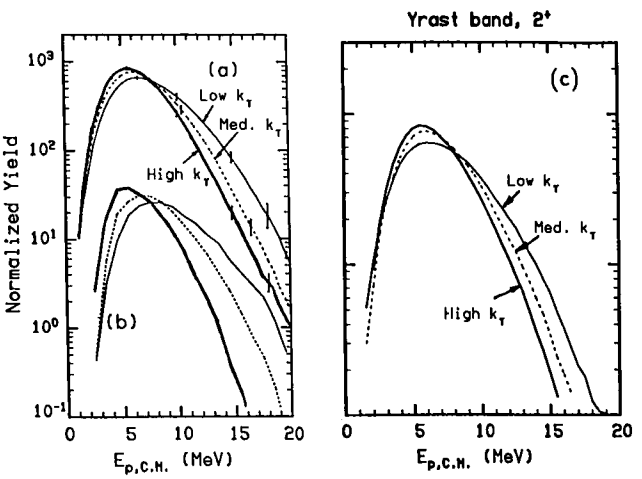

Figure 4. (a) Proton spectra coincident with the $2^+ \rightarrow 0^+$ transition in the ground band (band 3 in fig.3) of ^{82}Sr for the three k_γ gates indicated. The spectra are normalised to the same area for comparison. Typical statistical error bars are shown for selected bins. (b) Normalised theoretical proton spectra calculated with the evaporation code PACEX for the three γ-ray multiplicity gates corresponding approximately to the k_γ bins in (a). (c) shows the center-of-mass proton spectra coincident with the 2^+ level in band 4 (see fig.3) for the three k_γ gates. Here the proton emission barrier is essentially independent of the k_γ gating, although the high energy yield decreases as k_γ increases.

dominated by γ-rays from ^{82}Sr. Figure 3 shows a partial level scheme for ^{82}Sr constructed

from these data. Two new bands were established and four previously known bands were extended from 20 to 27 $\hbar$. The even parity band 4 is yrast for spins between 10 and 22 $\hbar$. The odd-spin band 2 becomes yrast for $I \geq 23$.

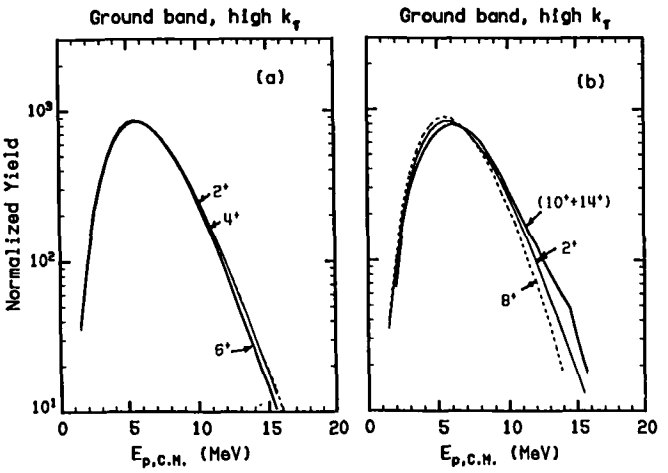

Figure 5. Panel (a) shows proton spectra coincident with γ-rays from the $2^+, 4^+$, and 6^+ levels in the ground band 3 for the high k_γ gate. The spectra are normalized to the same total counts for ease of comparison. The spectra are remarkably similar. Panel (b) shows proton spectra coincident with the 8^+ and the sum of $(10^+ + 14^+)$ levels in the same ground band 3 and for the high k_γ gate. The 2^+ spectrum is also shown for comparison. Significant differences are seen (see text).

Proton spectra coincident with the $2^+ \rightarrow 0^+$ ground transition are shown in fig. 4(a) for the three k_γ gates. For purposes of comparison, the spectra are shown normalized to the same total counts. As k_γ increases the most probable energy shifts to lower values and the spectra become narrower, but the high energy slopes (above ~15 MeV) for all k_γ gates are similar. This is understood in terms of the decreasing available thermal energy as k_γ or equivalently the spins of the entry region are increased (the three k_γ gates correspond to I~ 4–19, 17–29, and 26–45 $\hbar$, and to average yrast energies of ~7, 14 and 23 MeV, respectively). A statistical-model calculation with the evaporation code PACEX[18] for this system reproduces these features at least qualitatively. This is shown in fig. 4(b). In contrast to this, the proton spectra associated with the 2^+ level of band 4 (non-yrast at this spin, but yrast at spins 12 to 22$\hbar$) show similar peak positions for the three k_γ gates (fig. 4c). These differences in the spectra from two different 2^+ states suggest that some structural effects and/or feeding patterns may be responsible.

In order to explore any dependence of the proton emission probability on the structure of the final nucleus, we have compared in fig. 5(a) the proton spectra coincident with the γ-rays from the 2^+, 4^+, and 6^+ states in the ground band 3 and for the high k_γ gate. Clearly, the spectra are very similar. This is understood from the fact that the 2^+, the 4^+

and for the most part the 6^+ levels receive practically all their feeding from all the bands in ^{82}Sr.

In contrast, the 8^+ level in the same band 3 is fed from higher spin members of the ground band and to a significant fraction by the yrast band 4. Levels above the 8^+, however, are only populated by the decay of the levels of the continuation of the ground band. The proton spectra coincident with the 8^+ and the sum of 10^+ and 14^+ levels are compared in fig. 5(b) with the 2^+ spectrum. It is seen that the spectra for the 8^+ and $(10^+ + 14^+)$ levels have most probable values that shift toward lower and higher energies, respectively. These unexpected shifts are shown below to be consistent with the behavior of the spectra associated with the high spin states in the four major bands in ^{82}Sr.

If we further examine the proton spectra from individual levels within each band having spins higher than $10\hbar$ we find them to be similar to each other, but they differ considerably if they are associated with different bands. Thus, the proton spectra associated with transitions from the levels with spin 11, 13, and (19+23) in the odd spin band 2 of ^{82}Sr were found to be essentially identical in shape.

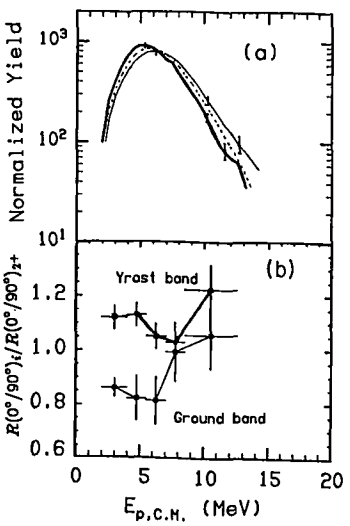

Figure 6. (a) Proton spectra coincident with the discrete transitions from the $(10^+ + 14^+)$ levels of the ground band 3 (thin line), the spin-13 level of the odd-spin band 2 (dashed line), and the $(14^+ + 16^+)$ levels of yrast band 4 (thick line) for the high-k_γ gate. (b) Ratio of the anisotropies of the protons for the high-spin levels of the ground band 2 (full squares and thin line) and of the yrast band 4 (solid squares and thick line) relative to the $2^+ \rightarrow 0^+$ ground-state transition for the high-k_γ gate. Vertical bars give statistical errors and horizontal ones the energy bins u sed for the angular distributions.

In contrast, when we compare proton spectra associated with high spin levels ($\geq 10\hbar$) at comparable excitation energies from different bands, large differences are found for all three k_γ gates. This is clearly seen in fig. 6(a), where proton spectra associated with the sum of the 10^+ and 14^+ levels in the ground band 3 (dashed line), the I=13 level of band 2 (thin line), and the sum of the 14^+ and 16^+ levels of the yrast band 4 (thick line) are shown for the high k_γ gate. The striking feature in these spectra is that for the same k_γ gate, the peak in the proton spectrum shifts down by 1 MeV in going from band 3 to

band 2 and then to the yrast band 4. This is comparable in magnitude to the shifts seen in fig. 4(a) for the $2^+ \rightarrow 0^+$ transition from the low to the high k_γ gate.

These results are surprising since the entry states are expected to lie at considerably higher excitation energies than the gating transitions and any correlation between the proton spectrum and the nature of the band being populated ought to be washed out by the statistical gamma emission. In fact, somewhat higher thermal energy is available for the yrast band 4 and this should shift its associated proton spectrum in the opposite direction. A possible explanation might be that although we have the same k_γ gate, the yrast band is populated from entry regions of higher spins compared to the ground or the other bands. This could cause a shift analogous to that in fig. 4(a).

We can offer a strong argument against the latter simple explanation in terms of phase-space effects. We note that the energy shifts are comparable to those for the $2^+ \rightarrow 0^+$ transition in fig. 4(a), where the spins and excitation energies for the three k_γ gates are greatly different. Consequently, a comparably large difference in the entry regions of the gating transitions should be easily observed experimentally by projecting the actual k_γ distributions coincident with the same discrete high spin transitions. We found that the k_γ distributions associated with the high spin discrete γ gates in the four bands are identical (the average k_γ values for the ground, odd spin, and yrast bands were found to be 15.5 ± 0.2, 15.5 ± 0.2 and 15.4 ± 0.2, respectively). In addition, a statistical model calculation in which the high multiplicity gate was moved up by one unit produced a considerably smaller shift in the proton spectrum than observed in fig. 6(a).

Another unlikely possibility would be that through fractionation the ground band samples the high total γ energy part of the entry region and the yrast band the lower one. This would give the yrast and ground bands less and more thermal energy, respectively. According to a statistical model calculation this does not affect the peak and sub-barrier portions of the proton spectra, but shifts the high energy part in the opposite direction than observed.

A reasonable explanation for the observed large shifts in the proton spectra is suggested by the steep experimental yrast line and consequently the entry line in ^{82}Sr and the energy balance in this reaction which places the entry line only a few MeV above the yrast line. This is also confirmed by statistical model calculations. These observations and the data suggest that a significant fraction of the population of the rotational bands in ^{82}Sr, and in particular the yrast band, occurs by direct proton emission from near-yrast states with the second proton playing that role. This mechanism could explain many features of the data and would in addition require that the last proton emission be stretched in character, particularly at and below the emission barrier, where it should exhibit a strong anisotropy $R(0°/90°) \equiv W(0°)/W(90°)$ with respect to the beam direction. This is indeed what we observe in fig. 6 where the anisotropy ratios for the high spin gates of fig. 3 of the ground and the yrast bands are plotted relative to the anisotropy of the $2^+ \rightarrow 0^+$ ground

transition as a function of the proton center-of-mass energy for the high k_γ gate. This further supports this explanation, since the direct population of the ground band has a higher Coulomb barrier compared to that for the population of the yrast band.

Additional support for this interpretation comes from statistical model calculations of the probability of the various decay sequences. In a spherical calculation we find that for $M_\gamma \geq 13$ the following paths receive the percentages in parentheses *nnpp* (25%), *npnp* (17%), *pnnp* (17%), *nppn* (12%), *pnpn* (13%), and *ppnn* (17%). Thus, 59% of the cascades leading to ^{82}Sr involve a proton as the fourth particle. In a calculation with deformation (assuming $\beta = 0.3$ for the nuclei with Z = 38, 39, and 40) the path percentages were *nnpp* (18%), *npnp* (14%), *pnnp* (16%), *nppn* (14%), *pnpn* (16%) and *ppnn* (22%), with 48% of the cascades leading to ^{82}Sr involving a proton as the fourth particle. A map of the population of the proton emitting states from the calculation with deformation is shown in fig. 7. The proximity of the proton emitting states to the yrast line supports the suggestion that a sizeable fraction of the emission of the proton as the fourth particle involves near yrast transitions.

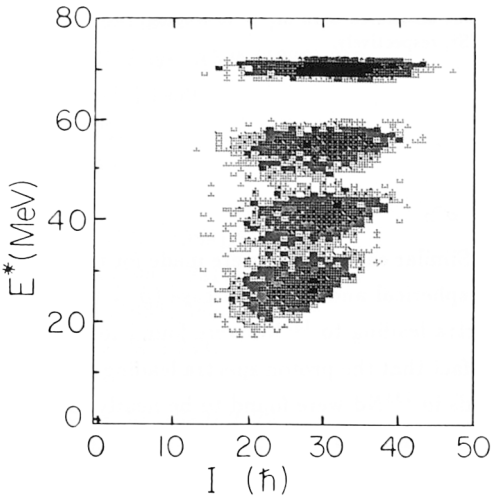

Figure 7. Population of the proton emitting states leading to ^{82}Sr following the reaction ^{52}Cr(^{34}S, 2n2p) at 130 MeV. The distribution is gated by requiring that $M_\gamma > 13$. It was calculated with the code PACEX assuming that the Z = 38,39, and 40 nuclei were deformed with $\beta = 0.3$. The separate regions correspond to regions in (E*, I) reached by the sequential particle emmision.

Next examine the sensitivity of the shape of the proton spectra to deformation effects based on the two calculations mentioned above. The results are summarized in fig. 8. The thick and thin curves in fig. 8 correspond to the spherical and deformed cases, respectively, for (a) all protons from the compound nucleus ^{86}Zr*, (b) for all protons leading to ^{82}Sr, and (c) for protons with $M_\gamma > 13$ leading to ^{82}Sr. It is seen that for all protons from ^{86}Zr*, the proton spectrum from the calculation with deformation shows a small increase in sub-barrier yield, which is noticeably smaller than what was found for the α spectra in the Yb systems (fig. 2). Furthermore, the proton spectra with deformation leading to ^{82}Sr [figs. 8(a) and 8(b)] show a decrease in the sub-barrier yield when compared to the

spherical case. This trend is in the opposite direction than expected. It can be shown that this is not due to an angular momentum effect because the spin distributions of the proton emitting states in the two calculations are similar. A likely explanation is that there are many competing channels with strengths altered when deformation is introduced in the calculation and this influences the channel selected spectra in the way seen in fig. 8. Because of such uncertainties arising in the calculated proton spectra, the channel selected spectra cannot be used as probes of deformation.

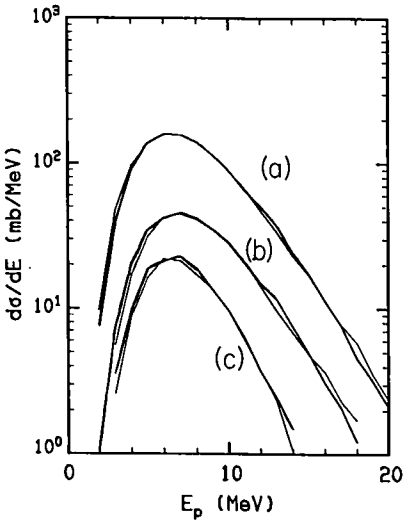

Figure 8. Proton spectra calculated for the reaction of 130 MeV ^{34}S with ^{52}Cr. The thin and thick lines correspond to calculations with a spherical and deformed optical model potential as in fig. 7. The curves (a),(b), and (c) are for all protons from ^{86}Zr, all protons leading to ^{82}Sr, and protons associated with $M_\gamma > 13$ leading to ^{82}Sr, respectively.

Similar calculations were made for the reaction ^{105}Pd(^{32}S, 2n2p)^{133}Nd at 155 MeV for the spherical and deformed case ($\beta = 0.4$ in the Z = 62,61, and 60 nuclei). The proton spectra leading to ^{133}Nd were found to be identical for the two cases. This may explain the fact that the proton spectra leading to the normal deformation and the superdeformed bands in ^{133}Nd were found to be nearly identical in shape.[30]

Returning to the ^{82}Sr case, proton emission from the near-yrast states may be associated with a predicted mechanism based on instability toward nucleon emission at large spins, connected with the population of $h_{11/2}$ resonance states in nuclei in this region.[29] These predicted yrast proton transitions were expected to have enhanced anisotropies as observed in our work.

In summary, we have observed a strong dependence of the proton energy spectra on the nature of the final high spin states belonging to different rotational bands in ^{82}Sr, which cannot be accounted for in terms of simple statistical model calculations that do not include explicitly nuclear structure effects. The large shifts toward lower energies and the stronger anisotropies when sub-barrier protons lead to high spin states in the yrast band compared to the ground band are interpreted as due to near-yrast emission of sub-barrier high-ℓ protons that preferentially populate the yrast band. These results suggest

that spectra and angular distributions of sub-barrier protons may provide a sensitive probe for connecting the population of the yrast band to the entry region.

At present it appears that the sub-barrier shape of the proton spectra does not reflect deformation effects in a clear way as in the case of the alpha spectra.

The authors acknowledge fruitful discussions with T. Døssing. M.A.R. and A.V. acknowledge support from the Joint Institute for Heavy Ion Research. This work was supported in part by the U.S. Department of Energy under grant No. DE–FG02–88ER–40406. Oak Ridge National Laboratory is operated by Martin Marietta Energy Systems Inc. under Contract No. DE–AC05–84OR21400 with the U.S. Department of Energy.

References

1) A.L. Goodman, *Nucl. Phys.* A352 (1981) 30.
2) A.L. Goodman, *Phys. Rev.* C37 (1988) 2162.
3) K.A. Snover, *Ann. Rev. Nucl. Part. Sci.*, 36 (1986) 545.
4) H.P. Morch *et al.*, *Phys. Rev. Lett.* 64 (1990) 1999 .
5) M. Blann and T.T. Komoto, *Phys. Scr.* 24 (1981) 93.
6) J.M. Alexander, D. Guerreau, and L.C. Vaz, *Z. Phys.* A305 (1982) 313.
7) F.A. Dilmanian *et al.*, *Phys. Rev. Lett.* 49 (1982) 1909.
8) Z. Majka *et al.*, *Phys. Rev. Lett.* 59 (1987) 322.
9) N.G. Nicolis *et al.*, *Phys. Rev.* C41 (1990) 2118.
10) Z. Majka *et al.*, *Phys. Rev.* C35 (1987) 2125.
11) N.G. Nicolis and D.G. Sarantites, *Phys. Rev.* **C40** (1989) 2422.
12) L.C. Vaz and J.M. Alexander, *Z. Phys.* **A318** (1984) 231.
13) M. Jääskeläinen *et al. Nucl. Instr. Meth.* 204 (1983) 385.
14) K.J. Honkanen *et al.*, *Nucl. Instr. Meth.* 257 (1987) 233.
15) La Rana *et al.*, *Phys. Rev.* C37 (1988) 1920 .
16) N.G. Nicolis and D.G. Sarantites, *Phys. Rev.* C40 (1989) 2422.
17) J.R. Huizenga *et al.*, *Phys. Rev.* C40 (1989) 668.
18) N.G. Nicolis *et al.* (unpublished).
18) A. Gavron, *Phys. Rev.* C21 (1980) 230; modification PACE2S by J.R. Beene (unpublished).
20) A. Bohr and B.R. Mottelson, Nucl. Structure (Benjamin, Reading, MA, 1975), Vol. II.
21) S.S. Hanna, in Giant Multipole Resonances, edited by F. Bertrand (Harwood, NY, 1980), Table I.
22) D. Wilmore and P.E. Hodgson, Nucl. Phys. 55 (1964) 673.
23) C.M. Perey and F.G. Perey, Nucl. Data Tables 17 (1976) 1.
24) L. McFadden and G.R. Satchler, Nucl. Phys. 84 (1966) 177.
25) B. Fornal *et al.*, *Phys. Rev.* C41 (1990) 127.

26) V.P. Aleshin, *J. Phys. G: Nucl. Part. Phys.* 16 (1990) 853.
27) W. Nazarewicz *et al.*, *Nucl. Phys.* A345 (1985) 319; private communication.
28) D.W. Stracener *et al.* Nucl. Instr. Meth. (in press). A CsI(Tℓ) version of the device described in: D.G. Sarantites *et al.* Nucl. Instr. Meth. A264 (1987) 319.
29) T. Dossing, S. Frauendorf, and H. Schulz, Nucl. Phys. A287 (1977) 137.
30) D. Ward *et al.*, this conference).